IOP PUBLISHING METROLOGIA

Metrologia **44** (2007) 505–512 doi:10.1088/0026-1394/44/6/010

Uncertainty budget for the NIST electron counting capacitance standard, ECCS-1*

Mark W Keller[1], Neil M Zimmerman[2] and Ali L Eichenberger[1,3]

[1] National Institute of Standards and Technology (NIST), 325 Broadway, Boulder, CO 80305-3328, USA
[2] National Institute of Standards and Technology (NIST), 100 Bureau Dr., Gaithersburg, MD 20899-8171, USA

E-mail: mark.keller@boulder.nist.gov, neil.zimmerman@nist.gov and Ali.Eichenberger@metas.ch

Received 19 September 2007
Published 21 November 2007
Online at stacks.iop.org/Met/44/505

Abstract
We measure a cryogenic, vacuum-gap capacitor by two methods: (1) charging it with a known number of electrons and measuring the resulting voltage, and (2) using a capacitance bridge traceable to the SI farad. We report a detailed uncertainty budget for the comparison of the two methods and find that they agree within a relative standard uncertainty of 9.2×10^{-7}. This comparison closes the quantum metrology triangle with the same uncertainty.

1. Introduction

The central principle of the electron counting capacitance standard (ECCS) is to realize directly the following definition of capacitance: given a pair of isolated conductors, moving a charge Q from one to the other creates a potential difference ΔU, and the ratio of these quantities is the capacitance, $C = Q/\Delta U$. In the ECCS, charge is moved as individual electrons, thus the value of C is intrinsically given in terms of the electron charge e. This can be contrasted with the current realization of the SI farad using the Thompson–Lampard calculable capacitor [1, 2]. In the latter approach, a device that closely approximates an ideal, infinite geometry yields a change in capacitance proportional to the displacement of a grounded guard electrode, with the constant of proportionality depending only on the electric constant, ε_0. A calculable capacitor gives a purely geometrical value of C (hence its name), while an ECCS depends fundamentally on the fact that charge is quantized in units of e. The main topic of this paper is the uncertainty budget for comparing measurements of the same capacitor using these two different methods. We also briefly discuss the implications for fundamental electrical standards of comparing a capacitance based on e with the SI farad.

Although the ECCS is simple in concept, counting electrons with the accuracy required for metrology is not an off-the-shelf technology. It requires the use of single-electron tunnelling (SET) devices, in which the transfer of individual electrons through tunnel junctions can be precisely controlled and monitored. These devices involve considerable technical complexity (at least for current incarnations), including the need for lithography at scales below 100 nm, temperatures below 0.1 K and sophisticated control of multiple gate signals with bandwidth of nearly 1 GHz. In return, they offer extraordinary performance: SET pumps can transfer individual electrons at rates of order 10 MHz with an error per cycle of order 10^{-9}, while SET electrometers can detect a small fraction of e and can have bandwidth of order 100 MHz. Reviews of the physics and applications of SET devices, and in particular detailed descriptions of how SET pumps and electrometers work, can be found in [3–5].

NIST has been working on components of the ECCS since the early 1990s. Operation of an initial prototype was reported in 1999, with a repeatability of order 10^{-7} but without a full uncertainty analysis [6]. The raw data considered here include two sets published in 1999 and a third set obtained using the same prototype, which we call ECCS-1. The completion of the uncertainty budget for these data was made possible by

* Official contribution of the National Institute of Standards and Technology; not subject to copyright in the United States.
[3] Current address: Federal Office of Metrology (METAS), Lindenweg 50, CH-3003 Bern-Wabern, Switzerland.

recent progress on determining the frequency dependence of the cryogenic capacitor used in the ECCS [7].

2. Including possible corrections to quantum electrical standards

Comparing an ECCS with the SI farad provides a powerful test of fundamental electrical metrology. Combined with previous work linking the calculable capacitor to the quantum Hall effect [8], it provides a way of closing the quantum metrology triangle [9, 10]. In this section we show how two possible corrections for quantum electrical standards enter into the equations for the ECCS.

The first possible correction involves the possibility that an SET device might not transfer a charge of exactly e in each cycle. We can express this by writing the actual transfered charge after N cycles as

$$Q = NQ_{\mathrm{S}} \qquad \text{with} \quad Q_{\mathrm{S}} = e(1+\varepsilon_S). \tag{1}$$

While it is generally expected that $\varepsilon_{\mathrm{S}} = 0$, there has been surprisingly little theoretical or experimental investigation of corrections to the SET charge quantum [11].

The second possible correction enters through the measurement of ΔU. The value of $C = NQ_{\mathrm{S}}/\Delta U$ found by counting electrons is not given directly in SI farads because we do not measure ΔU in SI volts. Instead, we use a Josephson voltage standard (JVS) [12] because it is the only readily available voltage standard with the required relative uncertainty ($< 10^{-7}$). A JVS driven at frequency f produces a voltage

$$U = \frac{nf}{K_{\mathrm{J}}} \qquad \text{with } K_{\mathrm{J}} = \frac{2e}{h}(1+\varepsilon_{\mathrm{J}}), \tag{2}$$

where n is an integer describing the step number of the array and h is the Planck constant. There are strong theoretical arguments for $\varepsilon_{\mathrm{J}} = 0$ and the universality of the Josephson effect has been demonstrated at the level of 10^{-10} or below [13, 14]. However, recent empirical tests based on the data for various fundamental constants put an upper bound on ε_{J} of a few parts in 10^7 [11, 15]. This value is larger than previously reported [14] because of inconsistencies in the input data.

The conversion of $NQ_{\mathrm{S}}/\Delta U$ to SI farads is straightforward. As is done routinely in modern electrical metrology, we use the value of the Josephson constant adopted by international agreement in 1990, $K_{\mathrm{J\text{-}90}} \equiv 483\,597.9\,\mathrm{GHz\,V^{-1}}$ [12]. The adoption of this value effectively established a 1990 volt, denoted by V_{90}, and this is the unit in which our calibrated voltmeter measures voltage. The relation between the 1990 volt and the SI volt is simply

$$\frac{\mathrm{V}_{90}}{\mathrm{V}} \equiv \frac{K_{\mathrm{J\text{-}90}}}{K_{\mathrm{J}}}. \tag{3}$$

Using this, and expressing a quantity X as the product of its numerical value and its unit, $X = \{X\}_{\mathrm{Y}}\mathrm{Y} = \{X\}_{\mathrm{Y}'}\mathrm{Y}'$, we can write

$$\frac{NQ_{\mathrm{S}}}{\Delta U} = \frac{NQ_{\mathrm{S}}}{\{\Delta U\}_{\mathrm{SI}}\mathrm{V}} = \frac{NQ_{\mathrm{S}}}{\{\Delta U\}_{90}\mathrm{V}_{90}} = \frac{NQ_{\mathrm{S}}K_{\mathrm{J}}}{\{\Delta U\}_{90}K_{\mathrm{J\text{-}90}}\mathrm{V}}. \tag{4}$$

Inserting Q_{S} and K_{J} from equations (1) and (2), we have the expression in SI farads,

$$\frac{NQ_{\mathrm{S}}}{\Delta U} = \frac{N(2e^2/h)}{\{\Delta U\}_{90}K_{\mathrm{J\text{-}90}}\mathrm{V}}(1+\varepsilon_{\mathrm{S}})(1+\varepsilon_{\mathrm{J}}), \tag{5}$$

where e and h have their usual SI values [14].

We now define C_{ECCS} as the value from equation (5) *assuming* $\varepsilon_{\mathrm{S}} = 0$ *and* $\varepsilon_{\mathrm{J}} = 0$, i.e.

$$C_{\mathrm{ECCS}} \equiv \frac{N(2e^2/h)}{\{\Delta U\}_{90}K_{\mathrm{J\text{-}90}}\mathrm{V}}. \tag{6}$$

We also define C_0 as the value measured directly in terms of the SI farad using a capacitance bridge traceable to a calculable capacitor. Setting this equal to equation (5) gives

$$C_0 = C_{\mathrm{ECCS}}(1+\varepsilon_{\mathrm{S}})(1+\varepsilon_{\mathrm{J}}). \tag{7}$$

Our experiment can then be expressed as a measurement of the ratio

$$\frac{C_0}{C_{\mathrm{ECCS}}} = (1+\varepsilon_{\mathrm{S}})(1+\varepsilon_{\mathrm{J}}) \approx 1+\varepsilon_{\mathrm{S}}+\varepsilon_{\mathrm{J}}, \tag{8}$$

where in the last step we have used the fact that both ε_{S} and ε_{J} are much less than 1. This is the quantity for which we calculate an uncertainty budget in this paper.

In the rest of this paper, we explain the operation of the ECCS in some detail and give a value and uncertainty budget for the ratio in equation (8). The implications of this result in light of the current status of the quantum metrology triangle are the focus of a separate paper [11].

3. Operation of the ECCS

The critical components of the ECCS are shown in figure 1(*a*). A 7-junction SET pump and an SET electrometer are fabricated on the same chip. The chip, two cryogenic needle switches (N1 and N2) and a vacuum-gap capacitor ($C_{\mathrm{cryo}} \approx 2$ pF) [16] are placed inside a metal box (with a separate enclosure for the capacitor). The box is connected to the mixing chamber of a dilution refrigerator and connections to room temperature are made with coaxial cables. The cryogenic switches allow multiple circuit configurations. With both switches closed, we can characterize the pump and electrometer using current versus voltage, current versus gate voltage and noise measurements. With N1 open, the small stray capacitance on chip allows us to determine the pump errors using a shuttle error measurement [17, 18]. Operation of the ECCS occurs in two phases, using the circuit configurations of figures 1(*a*) and (*b*).

3.1. Pumping phase

In the pumping phase, figure 1(*a*), we close N1 so that charge transferred by the SET pump goes onto the lower electrode of C_{cryo}. We open N2, which connects to a line running to room temperature, to avoid the large stray capacitance of this line. During the pumping phase, the voltage across the pump U_{p} must be kept near zero for two reasons: first, to avoid transfer errors in the pump [19], and second, to ensure that all charge transferred through the pump is placed on the desired capacitor rather than on the 10 pF stray capacitance to ground.

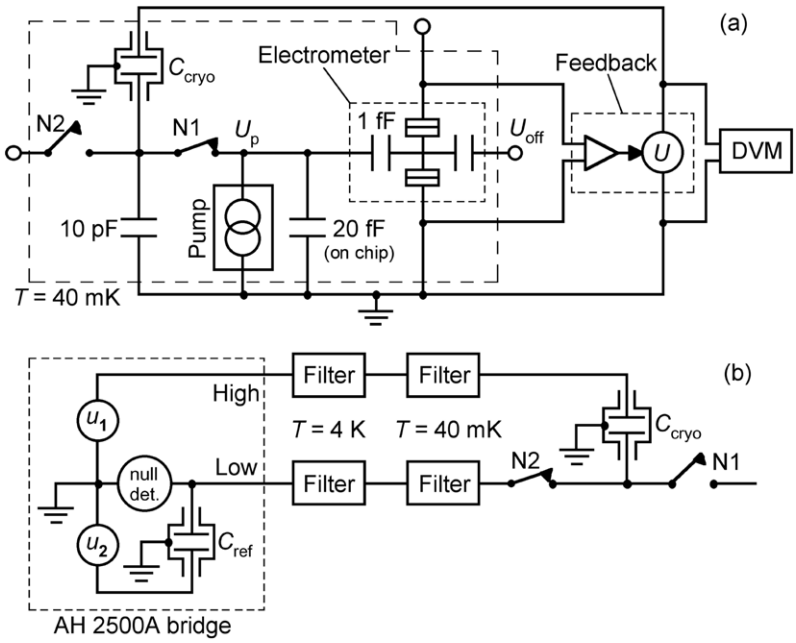

Figure 1. Schematic diagrams of the ECCS. (*a*) Configuration for the pumping phase. As charge is transferred through the pump onto C_{cryo}, the feedback (using the electrometer as a null detector) changes U in order to keep the voltage U_p fixed near 0. (*b*) Configuration for the bridge phase. With the ac voltages u_1 and u_2 adjusted to balance the bridge, $C_{cryo}/C_{ref} = u_2/u_1$.

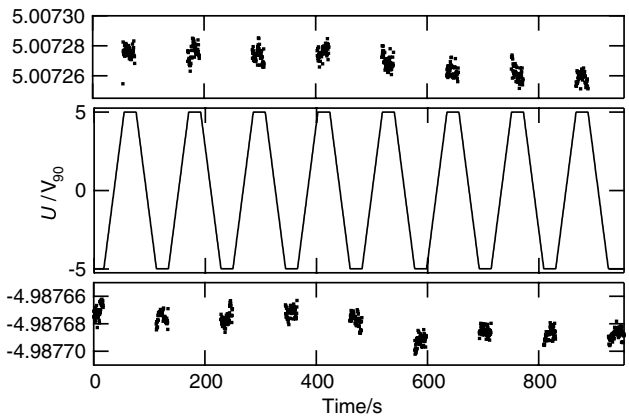

Figure 2. Feedback voltage U versus time during the pumping phase of the ECCS. Expanded views of the plateaux are shown above and below the main plot. These data are from Run I with $N = 114\,294\,785$ ($= 6D00001_{hex}$).

(This stray capacitance comes mostly from the grounded shell of C_{cryo}.) We accomplish this with a feedback circuit using the SET electrometer as a null detector. Any change in U_p results in a compensating voltage U applied to the upper electrode of C_{cryo}, thus keeping the island between the pump and the electrometer at virtual ground.

We record the feedback signal U using a digital voltmeter (DVM), and figure 2 shows a typical record of U versus time for repeated charging and discharging of C_{cryo}. The feedback must keep the pump voltage near zero at all times: when pumping starts in either direction, while charging C_{cryo} with $N \approx 10^8$ electrons to produce a voltage change $\Delta U \approx 10$ V, and when pumping stops to allow a measurement of U. Details of how we accomplish this, and how we verify that we are successful, are given in the appendix. The analysis of data such as those in figure 2, leading to the value for ΔU used in equation (6), is described in the next section.

3.2. Bridge phase

In the bridge phase, figure 1(*b*), we open N1 so that the SET components are disconnected from C_{cryo}, and close N2 to connect C_{cryo} to a capacitance bridge. We used an Andeen–Hagerling model 2500A bridge with option E [4] which operates at 1000 Hz. The coaxial cables connecting the bridge to C_{cryo} are relatively long (≈3 m each side) and have significant resistance, inductance and capacitance. In addition, there are 1 GHz low-pass filters at two locations on each cable (these are also present in the pumping phase and protect the SET devices from noise). The effect of these non-ideal cables on the bridge reading is discussed in section 5, but we note here that exchanging the high and low bridge leads did not affect the bridge reading. Since the bridge is traceable to the SI farad, the result of the bridge phase (after applying the loading correction described below) is C_0.

4. Uncertainties for the pumping phase

4.1. Type A uncertainty

For each data set such as that in figure 2 we determine a value of ΔU as follows. We calculate the mean value of U for each plateau and then compute the voltage change for each ramp up, ΔU_{pos}, and for each ramp down, ΔU_{neg} (both defined to be positive quantities). These differences are shown in figure 3, along with the mean values $\langle \Delta U_{pos} \rangle$ and $\langle \Delta U_{neg} \rangle$. We expect the mean values to be equal, and to the extent that

[4] The identification of specific commercial instruments does not imply endorsement by NIST nor does it imply that the instruments identified are the best available for a particular purpose.

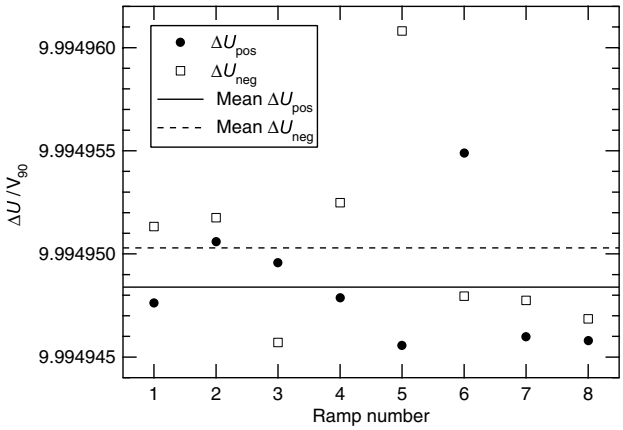

Figure 3. Voltage changes for ramping up, ΔU_{pos}, and for ramping down, ΔU_{neg}, for the data in figure 2. The lines show the mean values.

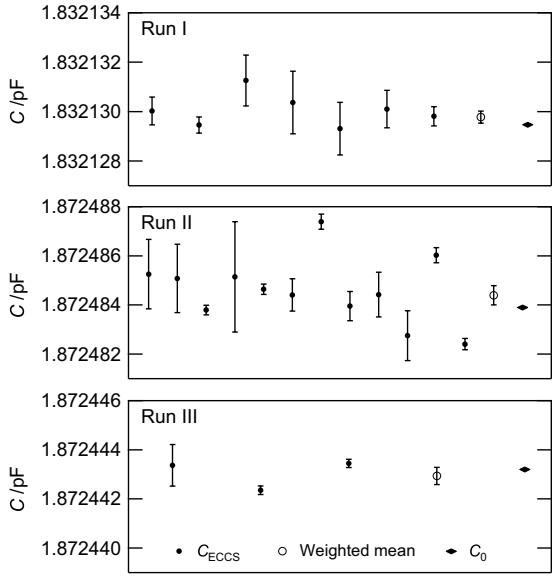

Figure 4. Capacitance values for each run of ECCS-1. Uncertainty bars for each value of C_{ECCS} and for the weighted mean are Type A only (see text). The bridge values C_0 discussed in section 5 are also shown, with their Type A uncertainty of 0.01×10^{-6} being smaller than the marker size in the plot.

they differ we assign a standard uncertainty due to asymmetry, $|\langle \Delta U_{\mathrm{pos}} \rangle - \langle \Delta U_{\mathrm{neg}} \rangle| \equiv 2\sigma_{\mathrm{asym}}$[5]. The final value of ΔU_i for the ith data set is simply the mean of all n_i values of ΔU (both positive and negative), and its standard uncertainty is the combination of σ_{asym} with the standard deviation of the mean (SDOM). Thus we have

$$\Delta U_i = \langle \Delta U \rangle_{n_i} \pm (\sigma_i^2/n_i + \sigma_{\mathrm{asym}}^2)^{1/2}, \qquad (9)$$

where σ_i is the standard deviation of the n_i values in the ith data set. The ith value of capacitance is found by inserting ΔU_i from equation (9) into equation (6).

A set of capacitance values obtained during an uninterrupted cooldown constitutes one 'run' of the ECCS (thermal cycling to room temperature changes the value of the cryogenic capacitor by as much as parts in 10^2). The data for all three runs of ECCS-1 are shown in figure 4. The bar on each point shows the uncertainty from equation (9), which we use as the weighting factor in computing the weighted mean for each run. We assign a Type A uncertainty to this weighted mean equal to the SDOM of the points in each run (see table 1). The bridge values for each run are also given in figure 4 for visual reference; a meaningful comparison requires consideration of the various Type B uncertainties discussed below.

A careful look at figure 4 reveals a key difference between the data for Runs I and III and those for Run II. For Run II only, the scatter for those points with the smallest uncertainty bars is much larger than one expects if the uncertainty given in equation (9) truly represents a standard uncertainty. The measurements in Run II span a period of about 10 days, whereas those for Runs I and III each span about 1 day. We believe the larger scatter in Run II is due to small instabilities in the dimensions of C_{cryo} that did not happen to occur during the shorter time span of Runs I and III. We know that C_{cryo} was not completely stable because on rare occasions we saw the value jump by large amounts (relative changes of order 10^{-5} to 10^{-4}, typically separated by more than a week). Given this, smaller changes during a period of 10 days are not surprising. Whatever the cause, the scatter seen in Run II is accounted for in our uncertainty budget by using the SDOM for the final Type A uncertainty.

[5] An asymmetry between ramping up and down can be caused by a small voltage across the pump. The details of this effect are described in [19].

4.2. *Type B uncertainties*

4.2.1. Voltmeter traceability to JVS. We measured U using a Hewlett-Packard 3458A DVM[4] that was calibrated by comparing directly with a JVS over the range ± 10 V in 1 V increments. This calibration has a relative standard uncertainty of 5×10^{-8} and was performed within two weeks of using the DVM with the ECCS. We recorded the internal temperature of the DVM to verify that it was near the calibration temperature and we ran its autocalibration routine daily to mimimize effects of drifts in internal components.

4.2.2. Leakage of C_{cryo}. To test whether charge placed on C_{cryo} could leak off through an unwanted conduction path, we charged to $U = \pm 10$ V and then monitored the feedback voltage for an hour or more. Data from such a test are shown in figure 5. In this case U moves slowly toward 0, as one expects for leakage, but we also observed cases where it drifted in the opposite direction and where it jumped suddenly in either direction. We believe these data are actually dominated by the $1/f$ noise of the electrometer, since similar drifts and jumps were observed near $U = 0$, but we can nevertheless use them to put an upper bound on the leakage effect. The dotted line in figure 5 is a linear fit to the data and has a slope of 6.5 nV s^{-1}. A change of e on C_{cryo} corresponds to a change in U of 90 nV, thus the dotted line represents a leakage rate of 0.07 e/s. (With 10 V across C_{cryo}, this implies a leakage resistance of 8.6×10^{20} Ω.) If this leakage were to persist during the entire 100 s of a ramp for $N = 2.5 \times 10^8$, it would represent a loss of 7e, or a relative change of $7/(2.5 \times 10^8) = 3 \times 10^{-8}$. We conservatively assign this as a relative standard uncertainty for leakage.

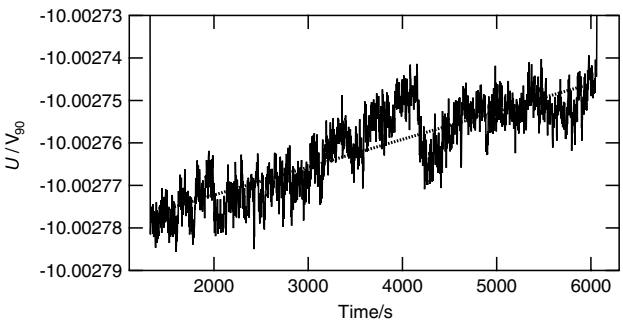

Figure 5. Data for testing leakage of C_{cryo} (see text).

4.2.3. Pump error. The shuttle error [18] of the 7-junction pump was measured once or twice a day and was typically 1×10^{-8}.

4.2.4. Miscellaneous. In equation (6) we use the 2002 CODATA recommended value of $h/e^2 = 25\,812.807\,449\,\Omega$, which has a relative standard uncertainty of 3.3×10^{-9} [14].

We have analysed the following effects for the pumping phase and estimated their uncertainties at well below 1×10^{-8}: thermal voltages in the coaxial cables, leakage of the coaxial cables, finite input impedance of the DVM. We also note that the very low effective frequency of charging in the pumping phase (period of order 100 s; see figure 2) means that loading corrections of the type described below in section 5.2.2 are negligible for the pumping phase.

5. Uncertainties for the bridge phase

5.1. Type A uncertainty

We used a bridge excitation voltage of 15 V_{rms} and averaged 256 samples to obtain each reading. We averaged 5 to 10 readings to obtain each bridge value, C_{bridge}, and the SDOM was typically 0.02 aF, so we assign a Type A relative standard uncertainty of 1×10^{-8} for the bridge phase.

5.2. Type B uncertainties

5.2.1. Bridge traceability to the SI farad. For our bridge measuring a value of 1.8 pF and using an excitation of 15 V_{rms}, the relative standard uncertainty specified by the manufacturer is 8.2×10^{-7}.[6] Although sufficient characterization of a particular bridge may allow one to go beyond this specification, during the operation of ECCS-1 we did not perform such measurements. We verified that our bridge was operating within specification by measuring 10 pF and 100 pF capacitors traceable to NIST's calcuable capacitor.

[6] Operation Manual for Andeen–Hagerling 2500A (with option E), Appendix C. According to the manufacturer, the expressions for uncertainties given in this appendix are for a coverage factor of four, i.e. they represent four times the standard uncertainty. The only significant component for our case is 'accuracy'; the uncertainties for linearity, temperature and stability are all negligible.

5.2.2. Loading corrections. Changes in the reading of a capacitance bridge due to properties of the cables between the bridge and the measured capacitor are collectively known as loading effects. These effects can be minimized by using short cables to reduce series resistance and inductance, and by using current equalizers to avoid poorly defined return current paths [20]. In our experiment, the cables connecting C_{cryo} to the bridge are less than ideal. They are about 3 m in length in order to reach the bottom of the cryostat and contain sections of brass and copper–nickel to provide thermal isolation. This results in each cable having a distributed resistance of a few ohms and a distributed inductance of a few microhenries. The filters shown in figure 1(*b*) consist of about 1 m of coiled wire surrounded by a mixture of epoxy and metal powder [21]. They contribute an additional resistance and inductance similar to that of the rest of the cable. Furthermore, we did not use current equalizers on the cables and the return current path included the grounded body of the cryostat. The result is that loading effects for our experiment are larger (and less well-understood) than is typical for precision capacitance measurements.

We quantified the loading effects by measuring C_{cryo} versus bridge frequency f at room temperature[7] with multiple values of extra resistance, inductance and capacitance added to the cables at the top, middle ($T = 4$ K) and bottom of the cryostat. Expressing the measured capacitance as

$$C_{\mathrm{bridge}} = A + Bf^2, \tag{10}$$

we consider the A and B terms separately. We found that B increased linearly with cable inductance and capacitance, and was independent of cable resistance, as expected for inductive voltage division [20]. For the cables without any added components, $B = 1.5 \times 10^{-12}\,\mathrm{pF\,Hz^{-2}}$, implying a loading effect on C_{bridge} at $f = 1000$ Hz of 1.5×10^{-6} pF. We therefore applied a loading correction to C_{bridge} in order to obtain the final value for the bridge phase,

$$C_0 = C_{\mathrm{bridge}} - 1.5 \times 10^{-6}\,\mathrm{pF}. \tag{11}$$

The relative standard uncertainty associated with this correction is 2.2×10^{-7}.

We found that A in equation (10) was unaffected by changes to the bridge High cable. For the Low cable, extra resistance decreased C_{bridge} and extra inductance increased C_{bridge}, although by small amounts in both cases. Since we do not fully understand the origin of these effects, we do not attempt to apply a correction for them. Instead, we account for them with an additional relative standard uncertainty of 2×10^{-7} in the budget for the bridge phase.

5.2.3. Cable leakage. We have considered cable leakage in the bridge phase and estimate that it contributes a relative uncertainty of order 10^{-10}.

6. Uncertainties in comparing the two phases

6.1. Frequency dependence of C_{cryo}.

Since the SET pump charges C_{cryo} at an effective frequency of order 0.01 Hz, while the bridge uses a sinusoidal excitation

[7] For these measurements we used an Andeen–Hagerling model 2700A variable-frequency bridge. It is very similar in operation to the 2500A and we expect very similar loading effects.

at 1000 Hz, we must consider whether C_{cryo} depends on frequency over this range. It is not possible to measure $C_{cryo}(f)$ directly down to 0.01 Hz, primarily because of the lack of any reference capacitor with a known frequency dependence in this range but also because of increasing null detector noise at low frequencies. However, an indirect approach has recently provided an upper bound for the change $C_{cryo}(1000\,\text{Hz}) - C_{cryo}(0.01\,\text{Hz})$ [7]. The observation that $C_{cryo}(f)$ measured above 100 Hz decreases rapidly with decreasing temperature is consistent with a model in which thin dielectric films on the surfaces of the electrodes are presumed responsible for the frequency dependence of a vacuum-gap capacitor. This model, when combined with surface measurements performed on the copper electrodes of C_{cryo} and previous data on properties of various dielectrics at low temperature, gives a relative standard uncertainty due to frequency dependence of 2×10^{-7}. Details of the analysis leading to this value are given in ref [7].

6.2. Voltage dependence of C_{cryo}

The attractive force between the electrodes of C_{cryo} increases with U, and could cause deformation leading to a dependence of the value of C_{cryo} on ΔU. Since the data in figure 4 include some values with $\Delta U = 10$ V and some with $\Delta U = 22$ V, and since the bridge uses a third voltage (15 V_{rms}), any such voltage dependence must be accounted for. We varied ΔU from 4 V to 22 V in the pumping phase and saw no change in C_{cryo}. These data (which appear in figure 4(*c*) of [6]) provide an upper bound on the voltage dependence and allow us to assign a relative standard uncertainty for this effect of 9×10^{-8}.

6.3. Motion of N1

The position of the switch N1 changes between the two phases of operation shown in figure 1, and this could affect the comparison between the phases. To test this, we measured C_{cryo} with the bridge at room temperature and moved the wire between N1 and C_{cryo} to simulate opening and closing N1. We saw no change within the noise of the measurement, giving a relative standard uncertainty for this effect of 1×10^{-7}.

7. Uncertainty budget

Table 1 summarizes the uncertainty components discussed above (excluding those below 1×10^{-8}). It also shows the combined uncertainty for all Type B sources and the total for each run.

8. Final result for C_0/C_{ECCS}

Figure 6 shows the comparison between C_{ECCS} and C_0 for each run in figure 4, expressed as the deviation from unity, $C_0/C_{ECCS} - 1$. The uncertainty bars in this plot include all the uncertainty components listed in table 1. The weighted mean of these data is

$$\frac{C_0}{C_{ECCS}} - 1 = (-0.10 \pm 0.92) \times 10^{-6}, \qquad (12)$$

with the final relative standard uncertainty being the combination of the 'Type B only' value in table 1 with the SDOM of the three data points. This result, showing no significant difference between C_{ECCS} and C_0, has two implications. First, from equation (8) we see that it puts an upper bound on possible corrections to the SET and Josephson effects, i.e. on the sum $\varepsilon_S + \varepsilon_J$, of 0.9×10^{-6}. Second, the established link between the calculable capacitor and the quantum Hall resistance with an uncertainty of a few parts in 10^8 [8] means that it also closes the quantum metrology triangle with an uncertainty of 0.9×10^{-6}. Understanding the implications of this for quantum electrical standards requires an examination of the current status of each of the individual 'legs' of the triangle; this discussion can be found in [11].

Table 1. Uncertainty budget for the ECCS. All values are relative standard uncertainties. The components are combined using the root-sum-square rule to give the totals at the bottom.

Component	Uncertainty/(μF F^{-1})
Pumping phase	
Type A	
Run I	0.13
Run II	0.21
Run III	0.19
DVM traceability to JVS	0.05
Leakage of C_{cryo}	0.03
Pump error	0.01
Bridge phase	
Type A	0.01
Bridge traceability to SI farad	0.82
Inductive loading correction	0.22
Other loading effects	0.2
Comparison between phases	
Frequency dependence of C_{cryo}	0.2
Voltage dependence of C_{cryo}	0.09
Motion of N1	0.1
Total (root-sum-square)	
Type B only	0.91
Run I	0.92
Run II	0.93
Run III	0.93

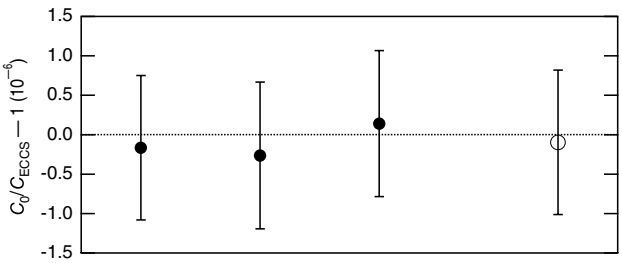

Figure 6. Solid circles: comparison between C_{ECCS} and C_0 for each run shown in figure 4. Open circle: weighted mean.

9. Conclusion

With the uncertainty budget reported here, the first comparison of a capacitance based on counting electrons with the SI farad is complete. Table 1 shows that the uncertainty is dominated by the traceability of the bridge, and we have recently performed measurements that should allow this component to be reduced

to 1 or 2 parts in 10^7. There are several components at about 2 parts in 10^7, and we believe they can each be reduced by a factor of 2 with modest effort. Finally, we are building a second generation of the ECCS that we expect will yield a Type A uncertainty for the pumping phase below 1×10^{-7}. Given all this, we expect the ECCS can achieve a total uncertainty of about 3×10^{-7}. With further experience, and more effort on the frequency dependence of C_{cryo}, it may eventually be possible to reduce the total uncertainty to 1×10^{-7} or below.

Acknowledgments

Clark Hamilton performed the DVM calibrations, Anne-Marie Jeffery provided the calibrated capacitors used to verify our capacitance bridge, and Yicheng Wang helped us understand various subtleties of the capacitance bridge measurements.

Each author contributed substantially to this work; MWK and ALE were the primary contributors to obtaining both the experimental data and the capacitance values; NMZ was the primary contributor to the systematic (Type B) uncertainty analysis.

Appendix A. Setup procedure for feedback in the pumping phase

The key to successful operation of the ECCS is keeping the voltage across the SET pump, U_{p}, close enough to zero that pump errors are negligible. For our 7-junction SET pumps, analysis of shuttle error data shows that the error per cycle does not change significantly for $|U_{\mathrm{p}}| < 20\,\mu\mathrm{V}$ (cf figure 7(*b*) of [22]). Based on simulations of pump errors described in figure 4 of [19], we have developed a sequence of steps designed to establish $U_{\mathrm{p}} = 0$, activate (lock) the feedback circuit without disturbing U_{p}, and finally test whether this condition is preserved after the feedback is locked. When the system passes this test the ECCS generally operates well.

(1) With the feedback disabled (and its output forced to zero by an internal switch), start the pump in the shuttle mode (pumping one electron back and forth repeatedly at a rate of order 1 MHz) and monitor the electrometer signal until it is stable. We cannot directly measure U_{p} in the configuration of figure 1(*a*), but we expect it to settle at the point where errors for forward and reverse pumping are equal, which is close to $U_{\mathrm{p}} = 0$ for pumps with fairly uniform junctions [19].

(2) Adjust the electrometer signal using the offset voltage U_{off} so that the input to the feedback is precisely nulled. This ensures that U will not jump when the feedback is locked. Such a jump could shift U_{p} away from the condition established in step 1. Further details about the effect of U_{off} can be found in [19].

(3) Stop the shuttle pumping and lock the feedback. The output U will now reflect the electrometer noise but it should not jump or drift monotonically in either direction.

(4) To test whether U_{p} remains near zero after the feedback has locked, we resume shuttle pumping. If U_{p} has moved significantly away from zero, the errors for forward and reverse pumping will no longer be equal. As the errors attempt to move U_{p} towards 0, the feedback will change U to compensate, resulting in a roughly linear drift in U with time. If such a drift is seen, we return to step 1.

(5) Stop shuttle pumping, configure the pump drive electronics to pump in one direction, and start pumping. Stop pumping when U reaches the desired starting voltage for operation of the ECCS, typically -5 V or -10 V.

(6) Repeat step 4 to confirm that U_{p} remains near zero.

(7) Configure the pump drive electronics to alternate between pumping N of order 10^8 electrons in either direction, with a wait period of order 10 s between directions, and start pumping. This will generate a U versus time trace similar to that in figure 2.

(8) When enough cycles of U versus time have been recorded, stop the pump during one of the wait periods. Step 4 can then be repeated to verify that U_{p} is still near zero.

The limit on how long the feedback can keep U_{p} near zero is set by background charge fluctuations in the electrometer. If a defect in the substrate moves and changes the electrometer island charge, the feedback will respond as if U_{p} had changed, thus shifting U_{p} away from the desired condition. Such a shift causes pump errors in one direction to increase [19], which results in a sudden increase in the asymmetry of $\langle \Delta U_{\mathrm{pos}} \rangle$ and $\langle \Delta U_{\mathrm{neg}} \rangle$. Operation of the ECCS must be stopped and the setup procedure described here performed again. For the prototype ECCS-1 discussed here, this effect limited continuous operation to approximately 1 h.

References

[1] Thompson A M and Lampard D G 1956 A new theorem in electrostatics and its application to calculable standards of capacitance *Nature* **177** 888

[2] Clothier W K 1965 A calculable standard of capacitance *Metrologia* **1** 36–55

[3] Averin D V and Likharev K K 1990 Single electronics: a correlated transfer of single electrons and Cooper pairs in systems of small tunnel junctions *Mesoscopic Phenomena in Solids* ed B L Al'tshuler *et al* (Amsterdam: Elsevier) pp 173–271

[4] Grabert H and Devoret M H (ed) 1992 *Single Charge Tunneling* (New York: Plenum)

[5] Likharev K K 1999 Single-electron devices and their applications *Proc. IEEE* **87** 606–32

[6] Keller M W, Eichenberger A L, Martinis J M and Zimmerman N M 1999 A capacitance standard based on counting electrons *Science* **285** 1706–9

[7] Zimmerman N M, Simonds B J and Wang Y 2006 An upper bound to the frequency dependence of the cryogenic vacuum-gap capacitor *Metrologia* **43** 383–8

[8] Jeffery A, Elmquist R E, Shields J Q, Lee L H, Cage M E, Shields S H and Dziuba R F 1998 Determination of the von Klitzing constant and the fine-structure constant through a comparison of the quantized Hall resistance and the ohm derived from the NIST calculable capacitor *Metrologia* **35** 83–96

[9] Likharev K K and Zorin A B 1985 Theory of Bloch-wave oscillations in small Josephson junctions *J. Low Temp. Phys.* **59** 347–82

[10] Piquemal F and Genevès G 2000 Argument for a direct realization of the quantum metrological triangle *Metrologia* **37** 207–11

[11] Keller M W 2007 Current status of the quantum metrology triangle *Metrologia* submitted

[12] Taylor B N and Witt T J 1989 New international electrical reference standards based on the Josephson and quantum Hall effects *Metrologia* **26** 47–62
[13] Mohr P J and Taylor B N 2000 CODATA recommended values of the fundamental physical constants: 1998 *Rev. Mod. Phys.* **72** 351–495
[14] Mohr P J and Taylor B N 2005 CODATA recommended values of the fundamental physical constants: 2002 *Rev. Mod. Phys.* **77** 1–107
[15] Mohr P J, Taylor B N and Newell D B 2008 CODATA recommended values of the fundamental physical constants: 2006, to be published
[16] Zimmerman N M 1996 Capacitors with very low loss: cryogenic vacuum-gap capacitors *IEEE Trans. Instrum. Meas.* **45** 841–6
[17] Keller M W, Martinis J M, Zimmerman N M and Steinbach A H 1996 Accuracy of electron counting using a 7-junction electron pump *Appl. Phys. Lett.* **69** 1804–6
[18] Kautz R L, Keller M W and Martinis J M 1999 Leakage and counting errors in a seven-junction electron pump *Phys. Rev.* B **60** 8199–212
[19] Jehl X, Keller M W, Kautz R L, Aumentado J and Martinis J M 2003 Counting errors in a voltage-biased electron pump *Phys. Rev.* B **67** 165331
[20] Kibble B P and Raynor G H 1984 *Coaxial AC Bridges* (Teddington, UK: NPL Management)
[21] Martinis J M, Devoret M H and Clarke J 1987 Experimental tests for the quantum behavior of a macroscopic degree of freedom: the phase difference across a Josephson junction *Phys. Rev.* B **35** 4682–98
[22] Keller M W 2001 Standards of current and capacitance based on single-electron tunneling devices *Recent Advanced in Metrology and Fundamental Constants, Proc. Int. School of Physics 'Enrico Fermi' (Varenna, Italy)* vol CXLVI ed T J Quinn *et al* (Amsterdam: IOS Press) pp 291–316